Article

Solvent-induced hysteresis loop in anionic spin crossover (SCO) isomorph complexes

Emmelyne Cuza,[a] Samia Benmansour,[b] Nathalie Cosquer,[a] Françoise Conan,[a] Carlos J. Gómez-García,[b]* Smail Triki[a]*

[a] Univ Brest, CNRS, CEMCA, 6 Avenue Le Gorgeu, C.S. 93837 - 29238 Brest Cedex 3, France;

[b] Instituto de Ciencia Molecular (ICMol). Departamento de Química Inorgánica. Universidad de Valencia. C/Catedrático José Beltrán 2. 46980 Paterna, Spain;

* Correspondence: smail.triki@univ-brest.fr, Tel.: +33-298-016-146; Carlos.Gomez@uv.es, Tel +34-963-544-423

Abstract: Reactions of Fe(II) with the tris-(pyridin-2-yl)ethoxymethane (py_3C-OEt) tripodal ligand in presence of the pseudohalide ancillary NCE^- (E = S, Se, BH_3) ligands led to a series of three mononuclear complexes formulated as $[Fe(py_3C\text{-}OEt)_2][Fe(py_3C\text{-}OEt)(NCE)_3]_2{\cdot}2CH_3CN$, with E = S (**1**), BH_3 (**2**) and Se (**3**). Single crystal characterizations (complexes **1**-**2**) and X-ray powder diffraction (complexes **1**-**3**) reveal monomeric isomorph structures formed by the spin crossover (*SCO*) anionic $[Fe(py_3C\text{-}OEt)(NCE)_3]^-$ complex, associated with the low spin (*LS*) cationic $[Fe(py_3C\text{-}OEt)_2]^{2+}$ complex and two solvent acetonitrile molecules. In the $[Fe(py_3C\text{-}OEt)_2]^{2+}$ cation, the Fe(II) is coordinated by two py_3C-OEt tridentate ligands, while the $[Fe(py_3C\text{-}OEt)(NCE)_3]^-$ anion displays a hexacoordinated environment involving three N-donor atoms of one py_3C-OEt ligand and three nitrogen atoms arising from of the three $(NCE)^-$ coligands. The magnetic studies show the presence of gradual *SCO* behavior for the three complexes: a one-step transition around 205 K for **1** and two step-transitions for compounds **2** and **3**, centred at 245 K and 380 K for **2**, and at 170 K and 298 K for **3**. The magnetic behaviors of complexes **1** and **2** remain unchanged when heating up to 500 K, while complex **3** shows significant changes which are caused by the crystallisation solvent loss above room temperature.

Keywords: Tripodal Ligands; pseudohalide coligands; Iron Complex; Spin crossover; Magnetic properties

1. Introduction

The spin crossover (*SCO*) complexes are by far the most studied molecular systems among switchable systems during the last decade thanks to their many potential applications, in particular for the development of new generations of electronic devices such as displays [1-4], memory devices [4-8], sensors [9-14], and Organic Light-Emitting Diodes (OLED) [15]. Although the *SCO* phenomenon can be essentially observed in octahedral complexes based on metal ions allowing spin state changes between the high spin (*HS*) and low spin (*LS*) states under external stimulus such as temperature, pressure, light irradiation or magnetic field, those based on Fe(II) ion exhibiting d^6 electronic configuration remain the most studied systems [16-35]. Nevertheless, such complexes are mostly either cationic or neutral, and the Fe(II) anionic complexes exhibiting *SCO* behavior are relatively very scarcely reported [27-35]. Furthermore, the few anionic *SCO* examples are restricted to only three different systems. The first one is the series $[Fe^{II}H_3L][Fe^{II}L]X$, (X^- = AsF_6^-, BF_4^-, ClO_4^-, PF_6^- and SbF_6^-), based on the ligand tris-(2-(((2-methylimidazol-4-yl)methylidene)amino) ethyl)amine (H_3L) and on its deprotonated anionic form (L^{3-}) [27]. The second one consists of the trinuclear $[Fe^{II}_3(\mu\text{-}L)_6(H_2O)_6]^{6-}$ complex involving the 4-(1,2,4-triazol-4-yl)ethanedisulfonate anion

Preprints (www.preprints.org) | NOT PEER-REVIEWED | Posted: 19 April 2021 doi:10.20944/preprints202104.0467.v1

(L^{2-}) [28], that displays a *HS-HS-HS* to *HS-LS-HS* transition above room temperature and a relatively large hysteresis loop (> 85 K). The last system concerns the series of mononuclear complexes based on the tripodal functionalized tris(2-pyridyl)methane (py_3C-R, R = C_nH_{2n+1}, aryl group, O-C_nH_{2n+1}, O-aryl, O-CO-C_nH_{2n+1}) ligands (Scheme 1a) [29-35]. Such complexes, of general formula $\{A[Fe((py_3C\text{-}R)(NCE)_3)]_m\}$ (A = $[(C_nH_{2n+1})_4N]^+$, $[Fe(py_3C\text{-}R)_2]^{2+}$, E = S, Se, BH_3), involve the $[Fe((py_3C\text{-}R)(NCE)_3)]^-$ anion generated by an Fe(II) metal centre, one py_3C-R chelating tripodal ligand and three terminal κN-SCE terminal coligands Scheme 1b). The different studies, reported essentially by Ishida et al. and some of us [29-35], concern essentially the study of the effect of the cationic counter-ion or the functional R group linked to the tripodal py_3C motif, on the *SCO* characteristics such as the transition temperatures and the cooperative effects. More recently, some of us extended such effects to the effect of the crystal packing through the design of a series of polymorph complexes [35].

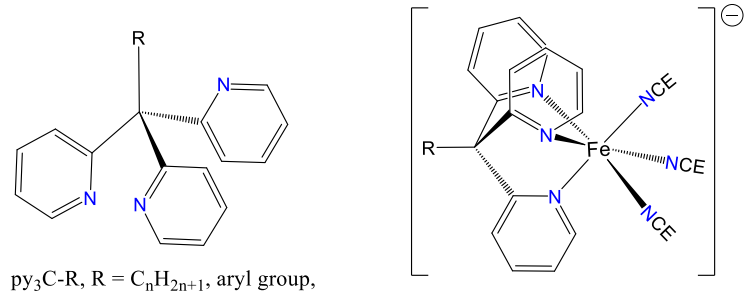

Scheme 1. (**a**) Examples of tris-(2-pyridyl)methane (py_3C-R) tripodal ligands and their principal coordination mode (**b**).

In order to determine the effect of the linear NCE^- (E = S, BH_3, Se) coligands on the *SCO* characteristics, we have reported recently two isomorph complexes of general formula, $[Fe(py_3C\text{-}OEt)_2][Fe(py_3C\text{-}OEt)(NCE)_3]_2.2CH_3CN$ (E^- = S, BH_3), based on the *SCO* $[Fe(py_3C\text{-}OEt)(NCE)_3]^-$ anion and on the cationic *LS* complex, $[Fe(py_3C\text{-}OEt)_2]^{2+}$, as counter-ion [34]. At the same time the $NCSe^-$ analogue complex (E = Se), that completes such isomorphic series, has been also prepared. However, this complex, of a presumably chemical formula of $[Fe(py_3C\text{-}OEt)_2][Fe(py_3C\text{-}OEt)(NCSe)_3]_2.2CH_3CN$ (**3**), could not be obtained as single crystals due to their instability. In addition, while magnetic behaviors of complexes **1** and **2** remain unchanged in the heating and cooling scan modes, complex **3** shows significant changes during the cooling/warming scan modes. These unexpected observations pushed us to explore in detail the peculiar switching behavior of this compound. In the present work, we report the syntheses, structural characterization, variable temperature infrared spectroscopy and magnetic properties of compound $[Fe(py_3C\text{-}OEt)_2][Fe(py_3C\text{-}OEt)(NCSe)_3]_2{\cdot}2CH_3CN$ (**3**) exhibiting solvent-induced hysteresis loop of 50 K, and the structural parameters at the origin of such peculiar magnetic behavior.

2. Results and Discussion

2.1. Syntheses

The tris-(pyridin-2-yl)ethoxymethane (py_3C-OEt) ligand was prepared as previously described [34-37]. Compound **3** was obtained as a red polycrystalline powder and as single crystals by mixing a solution of $[N(C_2H_5)_4](NCSe)$ with a solution of $FeCl_2$ and tris(pyridin-2-yl)ethoxymethane at -32 °C (see details in experimental section).

Preprints (www.preprints.org) | NOT PEER-REVIEWED | Posted: 19 April 2021 doi:10.20944/preprints202104.0467.v1

2.2. Structural Characterization and magnetic properties

In contrast to complexes **1** and **2** which have been structurally characterised by single crystal X-ray diffraction at room and low temperatures, complex **3**, that is expected to be isomorph to the structure observed for **1** and **2**, shows poor quality single crystal diffraction patterns that clearly precludes any correct single crystal structural characterization. However, after several attempts at 100 K, we succeeded in collecting some intensities, which led to unit cell parameters depicted in table 1. Comparison of these parameters to those of the two isomorph complexes **1** and **2**, indicates that the structure of complex **3** is isomorph to complexes **1** and **2** (Table 1). This conclusion was supported by the experimental X-ray powder diffraction pattern observed for the polycrystalline powder of complex **3**, which is very similar to the one observed for complex **1**, as well as to the simulated pattern derived from the single crystal structure of complex **1** (Figures 1 and S1).

Table 1. Crystal data of $[Fe(py_3C\text{-}OEt)_2][Fe(py_3C\text{-}OEt)(NCE)_3]_2\cdot 2CH_3CN$ (E = S (**1**), BH_3 (**2**), Se (**3**)).

	1		**2**	**3**
Temperature / K	293	100	200	100
Colour	Orange	Red	Red	Red
Formula	$C_{82}H_{74}Fe_3N_{20}O_4S_6$		$C_{82}H_{92}Fe_3N_{20}O_4B_6$	$C_{82}H_{74}Fe_3N_{20}O_4Se_6$
Space group	*P*-1		*P*-1	*P*-1
a /Å	11.6683(5)	11.432(5)	11.6827(8)	12.04(9)
b /Å	11.9026(7)	11.829(5)	12.0204(10)	12.29(9)
c /Å	17.1711(9)	16.857(5)	16.9162(11)	17.30(12)
α / °	78.192(5)	78.072(5)	78.389(6)	76.5(6)
β / °	88.279(4)	88.037(5)	87.805(6)	87.0(6)
γ / °	66.544(5)	65.879(5)	65.767(7)	64.2(7)
V / Å^3	2137.9(2)	2032.4(14)	2119.3(3)	2237(20)

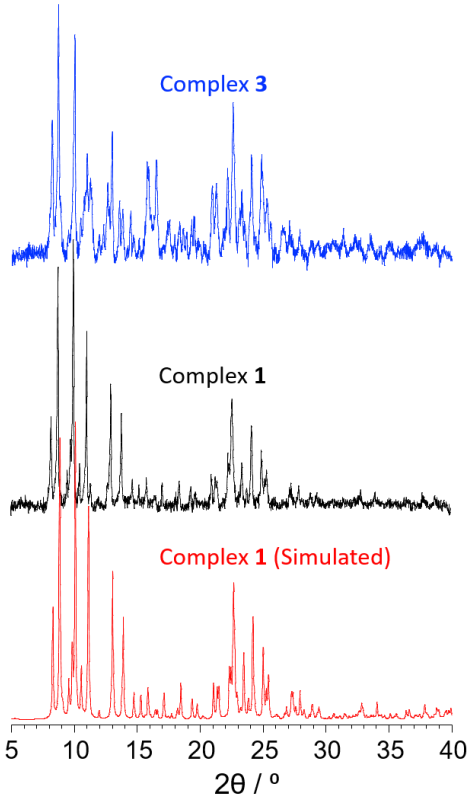

Figure 1. Experimental X-ray powder diffraction patterns for$[Fe(py_3C\text{-}OEt)_2][Fe(py_3C\text{-}OEt)(NCE)_3]_2\cdot 2CH_3CN$ (E = S (**1**), Se (**3**)), and the simulated one derived from the crystal structure of complex **1**.

Preprints (www.preprints.org) | NOT PEER-REVIEWED | Posted: 19 April 2021 doi:10.20944/preprints202104.0467.v1

It is also worth mentioning that the elemental analyses of complex **3** agrees with the chemical formula $[Fe(py_3C\text{-}OEt)_2][Fe(py_3C\text{-}OEt)(NCSe)_3]_2{\cdot}2CH_3CN$, expected for a complex isomorph to **1** and **2**. Therefore, all the data strongly support that the crystal structure of complex **3** is isomorph to those of complexes **1** and **2** [34]; and therefore its crystal structure consists of a low spin (LS) $[Fe(py_3C\text{-}OEt)_2]^{2+}$ cationic complex (Figure 2b), an anionic $[Fe(py_3C\text{-}OEt)(NCE)_3]^-$ (E = S (**1**), BH_3 (**2**) Se (**3**)) complex (Figure 2a) and two CH_3CN solvent molecules.

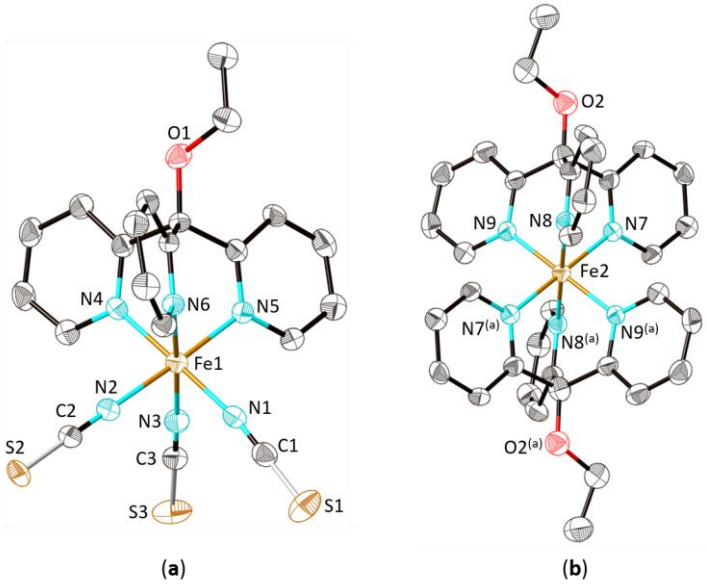

Figure 2. View of the anionic $[Fe(py_3C\text{-}OEt)(NCS)_3]^-$ (**a**) and of the cationic $[Fe(py_3C\text{-}OEt)_2]^{2+}$ (**b**) complexes in $[Fe(py_3C\text{-}Oet)_2][Fe(py_3C\text{-}OEt)(NCS)_3]_2{\cdot}2CH_3CN$ (**1**) [34]. Codes of equivalent positions: (a) = -x, -y, -z.

As previously described, complex **1** exhibits an incomplete *HS* to *LS* transition at $T_{1/2}$ = 205 K, while **2** displays a complete *HS* to *LS* two-step like transition centred at around 245 K and 380 K (Figure 3). For both complexes, the magnetic properties were measured in both cooling and warming modes (300-2-400-2 K for **1**; 300-2-500-2 K for **2**) but no significant hysteretic effects or any change due to possible desolvation were detected. Also, irradiation with a green laser at 10 K for several hours reveals no any noticeable increase of the magnetic moment in both samples. As for complex **1**, variable temperature susceptibility measurements were performed in the temperature range 300-5-400 K for complex **3**. The thermal variation of the product of the molar magnetic susceptibility times the temperature ($\chi_m T$) for the three complexes (**1**-**3**) are shown in Figure 3. The $\chi_m T$ values per formula (two Fe(II) ions) at 400 K for compound **3** (≈ 6.71 $cm^3\ K\ mol^{-1}$) corresponds to the expected values for two isolated metal ions with $S = 2$ and $g \approx 2.1$, indicating the presence of two magnetically isolated Fe(II) ions in the *HS* state ($S = 2$) [16-35]. On cooling, the $\chi_m T$ value of **3** shows a first abrupt drop, at around 298 K, reaching a value of *ca.* 3.40 $cm^3\ K\ mol^{-1}$ at 265 K. On further cooling, we can observe a second drop, at around 170 K, to reach a plateau at *ca.* 0.56 $cm^3\ K\ mol^{-1}$ below 116 K. This $\chi_m T$ value at low temperatures indicates the presence of a residual *HS* fraction of *ca.* 8 %. This behavior indicates the presence of an almost complete *HS* to *LS* two-step like transition centred at around 170 and 298 K.

In contrast to isomorphs **1** and **2**, where the magnetic properties do not show any change after successive cooling and heating scans in the ranges 2-400 K for **1** and 2-500 K for **2**, the two-step behavior described above for complex **3** (Figure 3) was only observed during the first cooling/heating cycle (300-5-400 K). Thus, the second cycle (400-50-400 K) in **3** produces a shift to lower temperatures for the first step while the transition temperature of the second step remains unchanged (See Figure S2). Similar trends were observed for the third and fourth cycles, until the fifth cycle where the initial first step merges with the second step, to lead to the gradual one step transition depicted in figure 4a.

Preprints (www.preprints.org) | NOT PEER-REVIEWED | Posted: 19 April 2021 doi:10.20944/preprints202104.0467.v1

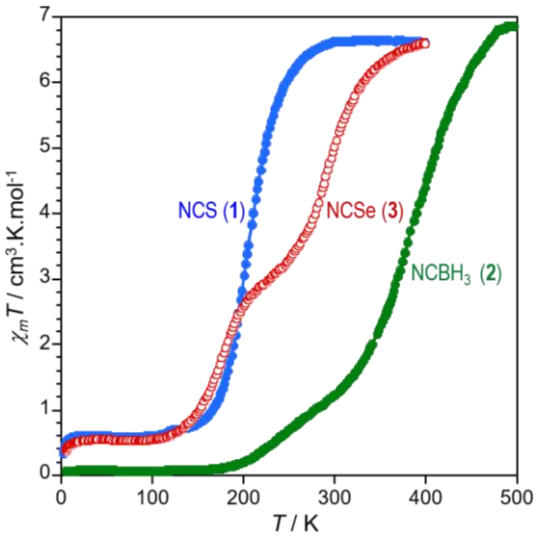

Figure 3. (**a**) Temperature dependence of the $\chi_m T$ product of **1** (●), **2** (●) and **3** (o)

It seems that heating the sample to 400 K produces a change which was probably induced by partial or total desolvation of the sample (see discussion below), but the *SCO* is still present. There are no hysteretic effects and the *HS* fraction of *ca.* 8 % remains unchanged after the different heating and cooling cycles.

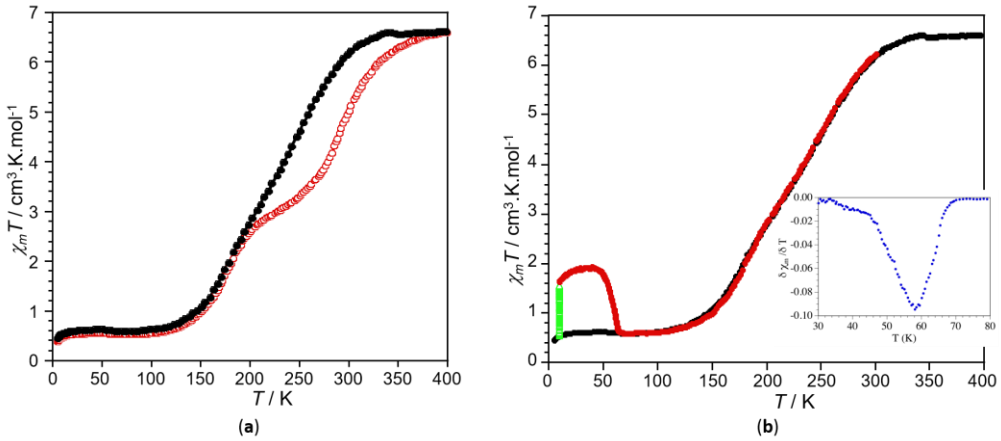

Figure 4. Magnetic properties of compound **3**: (**a**) Thermal variation of the $\chi_m T$ product for the solvated (o) and desolvated (●) samples; (**b**) thermal evolution of the $\chi_m T$ product for the desolvated sample in the dark (●), under 532 nm (Δ) light irradiation at 10 K and the subsequent thermal relaxation (●) in the dark. Inset shows the thermal variation of the derivative of $\chi_m T$ with temperature.

Irradiation of the sample at 10 K with a green laser (λ = 532 nm) produces an increase of the magnetic moment, indicative of the presence of a light-induced excited spin state trapping at low temperatures (LIESST effect). After *ca*. 4 h, the $\chi_m T$ product reaches saturation at a value of *ca*. 1.6 cm^3 K mol^{-1} (Figure S3). This value indicates that around 1/3 of one of the two LS Fe(II) centres in the $[Fe(py_3C\text{-}OEt)(NCS)_3]^-$ anions are excited to the *HS* state. After switching off the light irradiation, heating the sample further increases the $\chi_m T$ value up to *ca*. 2.0 cm^3 K mol^{-1} (representing *ca*. 44 % of one of the two Fe(II) centres). On further heating, the sample relaxes to the *LS* state at a T_{LIESST} of *ca*. 58 K (Figure 4b).

One of the major points, deserving special attention on the three isomorph complexes, concerns the origin of the unexpected and singular magnetic behavior that only occurs for isomorph **3** (see Figures 3 and 4a). To try to understand the process occurring at high temperature, we have

Preprints (www.preprints.org) | NOT PEER-REVIEWED | Posted: 19 April 2021 doi:10.20944/preprints202104.0467.v1

performed TGA analysis and X-ray powder diffraction on the three isomorphs to know more about the desolvation and solvation process of this system. Thus, TGA measurements were performed for the three isomorphs which were heated at 5 °C min^{-1}, under nitrogen atmosphere from room temperature to 390 K. In figure 5 are gathered the mass evolution with temperature for the three complexes, showing clearly that the two isomorphs **1** and **2** remain stable and retain their solvent molecules up to 390 K, while complex **3** starts to lose weight from room temperature and loses 4.37 % of its mass when heated up to 370 K, corresponding to two CH_3CN solvent molecules per formula unit. These measurements reveal that despite their isomorphic structures, complexes **1** and **2** retain their crystallization solvent molecules while complex **3** loses them even at moderate temperatures, suggesting that the crystal packing in **3** has larger cavities that allow an easy desolvation (see below).

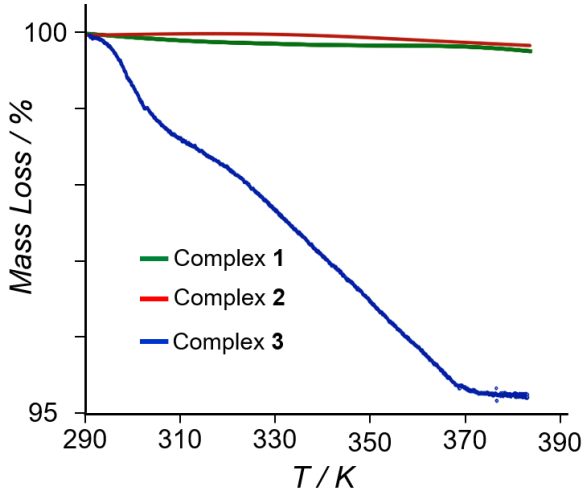

Figure 5. TGA analyses of compounds **1**-**3**.

To check for the reversibility of this desolvation process, we have performed successive desolvation and resolvation cycles, by heating the solvated sample and by adding two drops of CH_3CN on the desolvated sample, respectively. After resolvation, magnetic measurements (Figure S4) and X-ray powder diffraction (Figure 6) show that the sample has recover its original behavior, supporting the reversibility of the desolvation/resolvation process.

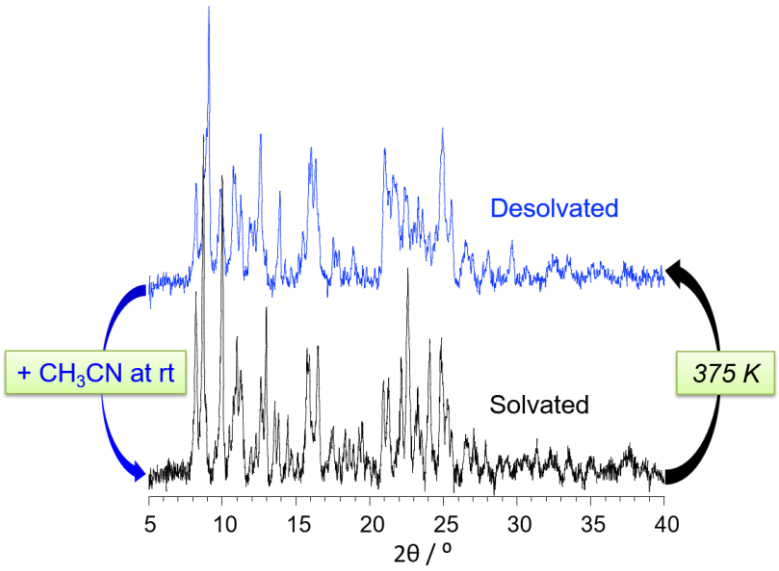

Figure 6. Experimental X-ray powder diffraction patterns of solvated and desolvated samples of **3**, confirming the reversibility of the desolvation/resolvation process.

Preprints (www.preprints.org) | NOT PEER-REVIEWED | Posted: 19 April 2021 doi:10.20944/preprints202104.0467.v1

2.3. Variable temperature magnetic properties and infrared spectroscopy

In order to confirm the Fe(II) spin state at high and low temperatures and the presence of the almost complete *HS* to *LS* transition for **3** with a residual *HS* fraction of *ca.* 8 % in the *LS* region (see Figure 3), we have measured the infrared spectrum at 100 and 300 K in the 1975-2130 cm^{-1} range, corresponding to the fundamental stretching vibration of the $NCSe^-$ units, since it is well known that the intensities of such stretching vibrations are very sensitive to the spin state of the Fe(II) metal ion [26, 34-35, 38-44]. Thus, we have recorded the infrared spectra for **3** at 350 and 100 K, according to the thermal evolution of the $\chi_m T$ product depicted in Figure 4a. The infrared spectra for **3** in the C≡N frequency region (1975-2130 cm^{-1}) at 350 and 100 K are displayed in Figure 7. At 350 K, two $\nu_{C\equiv N}$ stretching broad bands, characteristic of the *HS* state, appear at 2050 and 2075 cm^{-1}, while at 100 K, four strong bands, characteristic of the *LS* state, appear at 2044, 2075, 2082 and 2109 cm^{-1}. In agreement with the presence of a *HS* fraction of 8 % at low temperature (see magnetic section), the three bands observed at 2044, 2075, 2082 cm^{-1} can be viewed as resulting from the decrease in intensity of the two broad and strong bands observed for the *HS* state, while the band observed at higher frequency (2109 cm^{-1}) appears as the specific band of the *LS* state.

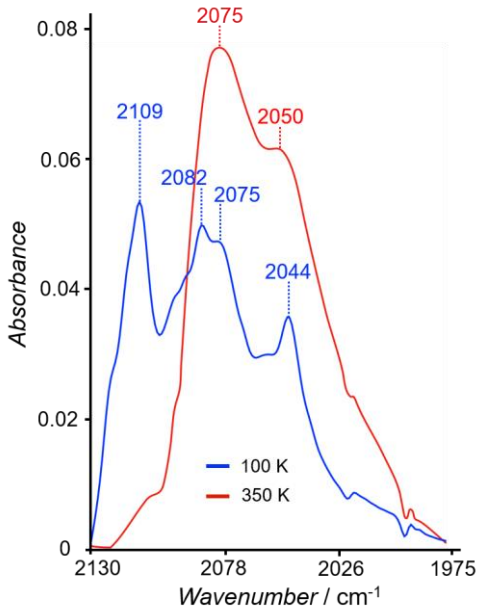

Figure 7. Infrared spectra for complex **3** in the 1975-2130 cm^{-1} region, showing the principal bands that are temperature sensitive.

2.4. Magneto-spectroscopic relationships

Based on the magnetic behaviors (Figure 4a) and on the main bands that are temperature sensitive (Figure 7) of both solvated and desolvated phases of complex **3**, we have investigated the thermal evolution of the infrared spectra of the stretching vibration of $NCSe^-$ in the range 1975-2130 cm^{-1}. For both phases (solvated and desolvated), we have recorded the infrared spectra in the vicinity of the *SCO* transitions from 100 to 350 K. First, we have recorded the infrared spectra for the freshly prepared complex **3** heating the sample from 100 to 350 K to avoid the partial desolvation of the sample (Figure 8a). Then, the same sample was heated during one hour at 400 K to ensure its complete desolvation, and the corresponding infrared spectra were then recorded cooling the sample from 350 to 100 K (Figure 8b).

Preprints (www.preprints.org) | NOT PEER-REVIEWED | Posted: 19 April 2021 doi:10.20944/preprints202104.0467.v1

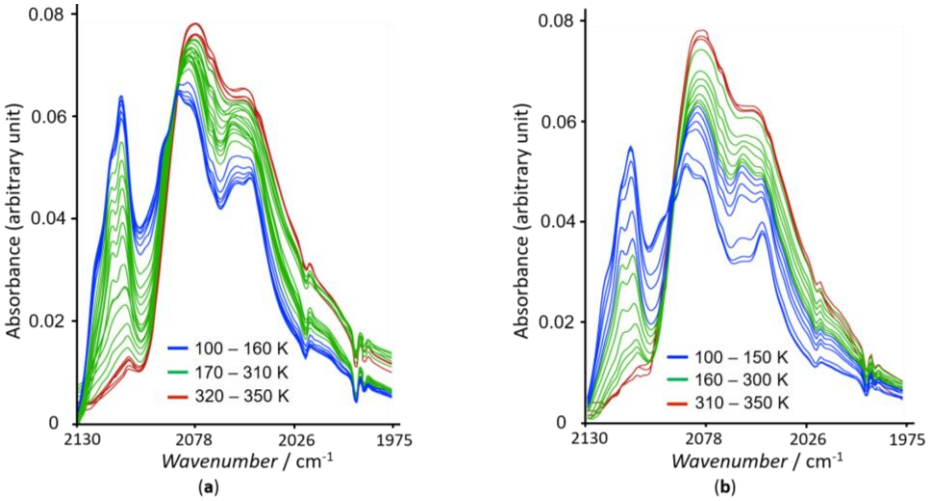

Figure 8. Temperature dependence of the infrared spectra in the temperature range 350-100 K, for compound **3:** solvated **(a)** and desolvated (**b**) samples.

The intensity of the two ν(NCSe) broad bands (2050 and 2075 cm^{-1}) characteristic of the *HS* state, gradually decreases with decreasing the temperature from 350 to 100 K but persists even at 100 K, supporting the presence of a fraction of *HS* Fe(II) centres, as revealed by the magnetic data. In parallel, a new band, characteristic of the *LS* state, appears at higher frequencies (2109 cm^{-1}) whose intensity gradually increases with decreasing the temperature. However, as can be easily observed in both Figures 8a and 8b, the infrared spectra did not show any clear difference between the infrared band evolutions of the solvated (Figure 8a) and desolvated (Figure 8b) phases of complex **3** as revealed by the magnetic data. Thus, in order to show more clearly this difference and to appreciate, at least qualitatively, the consistency of the experimental infrared data, we have correlated the thermal variation of the $\chi_m T$ product derived from magnetic study and the thermal evolution of the intensity of the infrared bands. The results, depicted in Figure 9, show an excellent correlation between the thermal evolution of the $\chi_m T$ product and that of the intensities of the characteristic infrared bands (2109, 2075, 2050 cm^{-1}), confirming the presence of a two-step *SCO* in the solvated sample (Figure 9a) but only a gradual one-step *SCO* in the desolvated sample (Figure 9b).

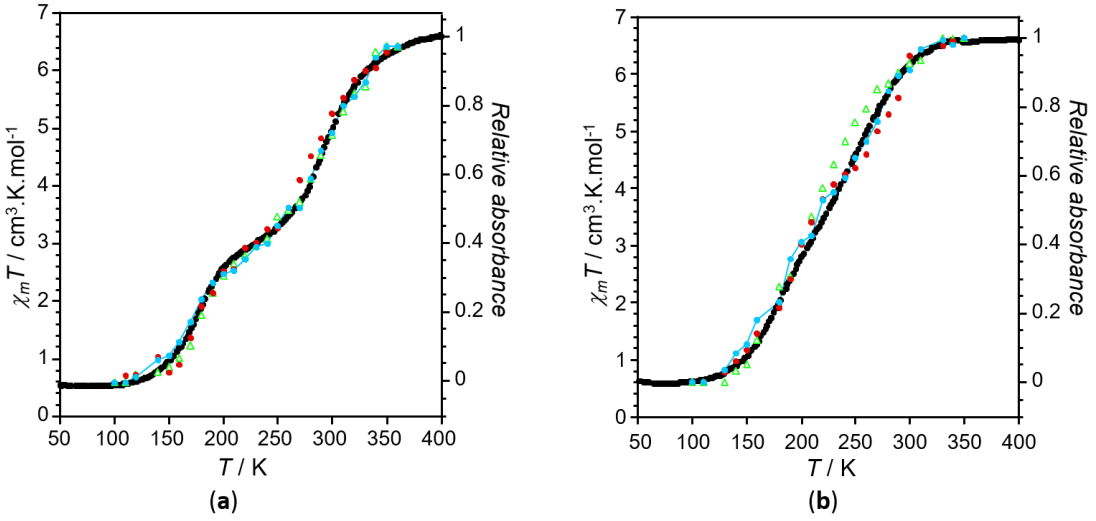

Figure 9. Temperature dependences of the $\chi_m T$ product and of the relative absorbance of the ν(CN) bands observed at 2109 cm^{-1} (Δ), 2075 cm^{-1} (●) and at 2050 cm^{-1} (-●-), for the solvated (**a**) and desolvated (**b**) samples of **3**.

Preprints (www.preprints.org) | NOT PEER-REVIEWED | Posted: 19 April 2021 doi:10.20944/preprints202104.0467.v1

The final question to be answered by this study is why the isomorph based on the $NCSe^-$ ligand (complex **3**) displays a reversible solvation/desolvation process with CH_3CN while the two other isomorphs (complexes **1** and **2**) retain the solvent molecules at temperatures exceeding 390 K. The answer can only come from the crystal packing of this triad of isomorphs. Indeed, examination of the crystal packing reveals that the CH_3CN solvent molecules are located in tetragonal-like channels running along the [010] direction, which are generated by eclipsed stacks of the -Fe-NCE…Fe…ECN-Fe-NCE…Fe- metallacycles (see Figure 10). Even if the three isomorphs display, as expected, similar crystal packing, the fact that they differ by the nature of the NCE^- ancillary ligands (E = S (**1**), BH_3 (**2**), Se (**3**)), induces strong differences in the sizes of the metallacycles, due to the different lengths of the three linear anions (the N-E distance increases from 2.72 Å for E = BH_3, to 2.80 Å for E = S and 2.94 Å for E = Se). The largest tetragonal-like channels are expected to be those of the isomorph with the longest ancillary linear ligand (i.e., compound **3**). Unfortunately, this difference could not be quantified due to the lack of single crystal structural data of complex **3**. However, in order to provide a reasonable estimation of the effect of the NCE^- ligands on the size of the metallacycles, we have calculated the relative increase of their dimensions when passing from complex **2** to complex **1** (see Figure 10 and Table 2 with the different Fe···Fe distances (d_1-d_4) determining the size of the channels).

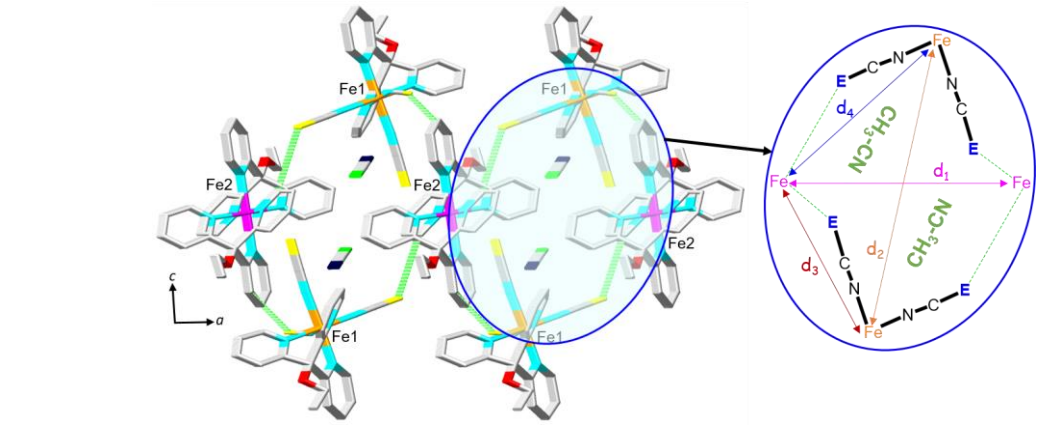

Figure 10. Structure and dimensions of the tetragonal-like channels where the CH_3CN molecules are located in compounds **1**-**3**.

As can be seen in Table 2, when passing from complex **2** (with $NCBH_3^-$ and N···B distance of 2.72 Å) to complex **1** (with NCS^- and N···S distance of 2.80 Å), there is an increase of +2.9 % in the size of the anion that leads to increases in the Fe···Fe distances in the metallacycle of up to 28.6 % (see d_1 to d_4 in Table 2). Therefore, if we consider complex **3** based on the $NCSe^-$ linear ligand that corresponds to the biggest linear anion (with N···Se distance of 2.94 Å), the expected metallacycle should be significantly larger than those observed for the isomorphs **1** and **2**. These observations explain clearly why complex **3** involves larger tetragonal-like channels allowing the easy and reversible solvation and desolvation processes.

Table 2. Relative increase Fe…Fe distances (d_1 and d_2) as function of the nature of the NCE^- ancillary ligands ($d_{N\cdots E}$) in the two isomorphs **1** and **2**.

	2 (E = BH_3)	**1** (E = S)	**3** (E = Se)
$d_{N\cdots E}$ (relative increase)	2.72 Å	2.80 Å (+2.9 %)	2.94 Å (+8.1 %)
T / Spin State	200 K / *LS*	100 K / *LS*	–
d_1 (relative increase)	12.757	14.774 Å (+15.8 %)	–
d_2 (relative increase)	11.683 Å	12.653 Å (+8.3 %)	–
d_3 (relative increase)	8.146 Å	10.481 Å (+28.6 %)	–
d_4 (relative decrease)	9.125 Å	8.907 Å (-2.4 %)	–

Preprints (www.preprints.org) | NOT PEER-REVIEWED | Posted: 19 April 2021 doi:10.20944/preprints202104.0467.v1

3. Experimental Section

3.1. Starting Materials

All starting reagents and solvents were purchased and used as received (Sigma-Aldrich, Acros Organic, Cambridge Isotope Laboratories). All the organic syntheses were performed under nitrogen atmosphere. The tris-(pyridin-2-yl)ethoxymethane (py$_3$C-OEt) ligand was prepared as previously described [36,37], with slight modifications to increase the chemical yield [34,35].

*3.2. Synthesis of [Fe(py$_3$C-OEt)$_2$][Fe(py$_3$C-OEt)(NCSe)$_3$]$_2$·2CH$_3$CN (**3**)*

In 5 mL of distilled methanol were dissolved tris-(pyridin-2-yl)ethoxymethane (50.0 mg, 0.17 mmol), iron(II) chloride anhydrous salt (20.0 mg, 0.16 mmol) and few mg of ascorbic acid. The resulting solution was stirred for 15 minutes at room temperature and then a solution of acetonitrile (5 mL) containing 0.69 mmol of [(C$_2$H$_5$)$_4$N](NCSe) was added. The resulting solution was stirred for 30 minutes, filtered and quickly cooled at -32 °C. After three days bright red micro-crystalline powder of (**3**) as well as red single crystals were recovered. Anal. Calcd. (%) for [Fe(py$_3$C-OEt)$_2$][Fe(py$_3$C-OEt)(NCSe)$_3$]$_2$·2CH$_3$CN (C$_{82}$H$_{74}$Fe$_3$N$_{20}$O$_4$Se$_6$) **3**: C, 48.2; H, 3.7; N, 13.7; Found (%): C, 47.9; H, 3.8; N, 14.0. IR data (ν/cm^{-1}) for the freshly filtered sample (powder and single crystals, Figure S5): 410 (w), 423 (w), 477 (w), 500 (w), 513 (w), 530 (w), 659 (m), 726 (w), 758 (w), 886 (w), 1011 (m), 1086 (w), 1108 (m), 1143 (m), 1205 (w), 1252 (w), 1291 (w), 1389 (w), 1434 (m), 1462 (s), 1593 (m), 2060 (s), 2244 (w), 2871 (w), 2901 (w), 2972.11 (w), 3076 (w), 3442 (br).

3.3. Characterization of the Materials

Infrared spectra of complex **3** have been performed at room temperature, in the 4000-400 cm^{-1} range, using a platinum ATR Vertex 70 BRUKER spectrometer. Temperature dependence of the IR spectra was performed in the 2130-1975 cm^{-1} range, using a Vertex 70 BRUKER spectrometer with variable temperature cell holder (VT Cell Holder typer P/N GS21525). The IR data have been qualitatively analyzed in the form of absorbance (ABS) *vs.* wavenumber (in cm^{-1}). For the quantitative analysis and comparison with the thermo-magnetic and photo-magnetic measurements, the intensities of the *HS* vibration bands were represented as ABS *vs. T*, while the intensities of the *LS* vibration bands were represented as (1-ABS) *vs. T*. All NMR spectra (^{1}H et ^{13}C) were performed using BRUKER DRX 300 MHz, Advance 400 MHz and Advance III HD 500 MHz equipment. All chemical shifts are defined in ppm and determined by using the rightful deuterated solvent as a reference. TGA measurements were performed on ATG-LabsysTM, Setaram. The sample was preliminary put under vacuum and then heated at 5°C.min^{-1} under nitrogen atmosphere.

3.4. Magnetic Measurements

Magnetic susceptibility measurements were carried out in the temperature range 2-400 K with an applied magnetic field of 0.1 T, on a polycrystalline sample of **3** (with a mass of 5.896 mg) with a Quantum Design MPMS-XL-5 SQUID susceptometer (San Diego, CA, USA). The susceptibility data were corrected for the sample holders previously measured using the same conditions and for the diamagnetic contributions of the salt as deduced by using Pascal's constant tables [45]. The photomagnetic studies were performed by cooling the samples down to 10 K at a rate of 1 K min^{-1} and then irradiating them with a green Diode Pumped Solid State Laser DPSS-532-20 from Chylas (λ = 532 nm, power = 20 mW) coupled *via* an optical fibre to the cavity of the SQUID magnetometer. When saturation of the magnetization was reached (after *ca*. 4 hours), the laser was switched off and the sample was heated up to 300 K at a rate of 0.4 K min^{-1}. The sample for the LIESST studies consisted of a thin layer of microcrystalline powder of compound **3**.

4. Conclusions

We have shown that the compound $[Fe(py_3C\text{-}OEt)_2][Fe(py_3C\text{-}OEt)(NCSe)_3]_2{\cdot}2CH_3CN$ (**3**), based on the $[Fe(py_3C\text{-}OEt)_2]^{2+}$ *LS* cation and the *SCO* $[Fe(py_3C\text{-}OEt)(NCSe)_3]^-$ anion, displays a reversible desolvation process that affects the *SCO* behavior. This compound has been prepared as polycrystalline powder and as single crystals using a similar protocol than that used previously for the syntheses of the two isomorphic complexes $[Fe(py_3C\text{-}OEt)_2][Fe(py_3C\text{-}OEt)(NCE)_3]_2{\cdot}2CH_3CN$ (E = S (**1**), BH_3 (**2**)) based on the two ancillary linear ligands NCS^- and $NCBH_3^-$ [34]. Despite being obtained in the form of prismatic-shaped single crystals, complex **3** could not be characterized by X-ray single crystal diffraction, because of the low stability of its single crystals, in contrast to complexes **1** and **2** which have been structurally characterized. However, combined X-ray powder diffraction, infrared spectra and CHN elemental analyses clearly revealed that complex **3** exhibits an isomorph structure than that of complexes **1** and **2**. TGA analyses performed on the single crystal samples of the three isomorphs revealed clearly that the two isomorphs **1** and **2**, for which the corresponding single crystals are stable, retain their solvent molecules up to 390 K, while complex **3** begins to lose its CH_3CN solvent molecules from room temperature. The magnetic studies for **3** performed in cooling and heating scans in the temperature ranges 300-5 K and 5-400 K, respectively, indicate the presence of an incomplete *HS* to *LS* two-step like transition centred around 170 and 298 K, while when the sample was heated at 400 K until its complete desolvation, the magnetic behavior of the high temperature transition ($T_{1/2}$ = 298 K) shifts to lower temperature until the two-step behavior merges with a gradual one-step transition at *ca.* 216 K. Such behavior which can be viewed as a solvent-induced hysteresis loop of 50 K [46], was confirmed by infrared spectra recorded in the vicinity of the *SCO* transition for both solvated and desolvated samples. Furthermore, successive desolvation and solvation cycles, tracked by SQUID measurements and X-ray powder diffraction, show that the desolvation process is fully reversible. As shown by the TGA analysis, compound **3** exhibits a different magnetic behavior due to its easy desolvation and solvation process, in contrast to the two other isomorphs that retain their solvent molecule up to 390 K, despite their isomorph structures. This unexpected behavior was elucidated by careful examination of the crystal packing of these isomorph complexes, which clearly revealed that the solvent molecules are located in tetragonal-like channels generated by the eclipsed stacks of the "-Fe-NCE…Fe…ECN-Fe-NCE…Fe-" metallacycles. Therefore, the isomorph based on the bigger $NCSe^-$ ancillary ligand, should display the larger tetragonal-like channels, allowing easier solvation and desolvation as observed in isomorph **3**.

Author Contributions: E.C. synthesized the ligand and the complex with supervision of S.T.; and recorded and analysed the infrared spectra with supervision of N.C. and S.T.; F.C. supervised the organic syntheses and interpreted the NMR spectra; S.B. performed the X-ray powder diffraction; C.J.G.G performed and interpreted the magnetic measurements; S.T. supervised the experimental work and wrote the manuscript on which all the authors have contributed.

Funding: This research was funded by the French CNRS (MITI Project), Mol-CoSM ANR Project N° ANR-20-CE07-0028-01 the "Université de Brest" (IBSAM institute), the Région Bretagne (EC), the Generalidad Valenciana (Prometeo2019/076 project) and the Spanish MINECO (Project CTQ2017-87201-P AEI/FEDER, EU).

Conflicts of Interest: The authors declare no conflict of interest.

References

1. Cobo, S.; Molnár, G.; Real, J.-A.; Bousseksou, A. Multilayer Sequential Assembly of Thin Films That Display Room-Temperature Spin Crossover with Hysteresis. *Angew. Chem. Int. Ed.* **2006**, *45*, 5786–5789.

2. Kahn, O.; Martinez, C. J. Spin-transition polymers: from molecular materials toward memory devices. *Science* **1998**, 279, 44–48.

3. Garcia, Y.; van Koningsbruggen, P. J.; Codjovi, E.; Lapouyade, R.; Kahn, O.; Rabardel, L. Non-classical FeII spin-crossover behaviour leading to an unprecedented extremely large apparent thermal hysteresis of 270 K: application for displays. *J. Mater. Chem.* **1997**, *7*, 857–858.
4. Murray, K.S.; Kepert, C.J. Cooperativity in Spin Crossover Systems: Memory, Magnetism and Microporosity. *Top. Curr. Chem.* **2004**, *233*, 195-228.
5. Létard, J.-F.; Guionneau, P.; Goux-Capes, L. Towards Spin Crossover Applications.*Top. Curr. Chem.* **2004**, *235*, 221–249.
6. Bousseksou, A.; Molnar, G.; Salmon, L.; Nicolazzi, W. Molecular spin crossover phenomenon: recent achievements and prospects. *Chem. Soc. Rev.* **2011**, *40*, 3313-3335.
7. Rueckes, T.; Kim, K.; Joselevich, E.; Tseng, G. Y.; Cheung, C.-L.; Lieber, C. M. Carbon Nanotube-Based Nonvolatile Random Access Memory for Molecular Computing. *Science* **2000**, *289*, 94-97.
8. Galet, A.; Gaspar, A. B.; Carmen Muñoz, M.; Bukin, G. V.; Levchenko, G.; Real, J.-A. Tunable Bistability in a Three-Dimensional Spin-Crossover Sensory- and Memory-Functional Material. *Adv. Mater.* **2005**, *17*, 2949–2953.
9. Bartual-Murgui, C.; Akou, A.; Thibault, C.; Molnar, G.; Vieu, C.; Salmon, L.; Bousseksou, A. Spin-crossover metal–organic frameworks: promising materials for designing gas sensors. *J. Mater. Chem. C*, **2015**, *3*, 1277–1285.
10. Lapresta-Fernandez, A.; Titos-Padilla, S.; Herrera, J. M.; Salinas-Castillo, A.; Colacio, E.; Capitan-Vallvey, L. F. Photographing the synergy between magnetic and colour properties in spin crossover material [Fe $(NH_2trz)_3$]$(BF_4)_2$: a temperature sensor perspective. *Chem. Commun.* **2013**, *49*, 288–290.
11. Linares, J.; Codjovi, E.; Garcia, Y. Pressure and temperature spin crossover sensors with optical detection. *Sensors* **2012**, 12, 4479–4492.
12. Cuéllar, M. P.; Lapresta-Fernández, A.; Herrera, J. M.; Salinas-Castillo, A.; Pegalajar, M. del C.; Titos-Padilla, S.; Colacio, E.; Capitán-Vallvey, L. F. Thermochromic sensor design based on Fe (II) spin crossover/polymers hybrid materials and artificial neural networks as a tool in modelling. *Sensors and Actuators B*, **2015**, *208*, 180–187.
13. Rodriguez-Jimenez, S.; Feltham, H. L. C.; Brooker, S. Non-Porous Iron(II)-Based Sensor: Crystallographic Insights into a Cycle of Colorful Guest-Induced Topotactic Transformations. *Angew. Chem. Int. Ed.* **2016**,55, 15067–15071.
14. Benaicha, B.; Van Do, K.; Yangui, A.; Pittala, N.; Lusson, A.; Sy, M.; Bouchez, G.; Fourati, H.; Gómez-García, C. J.; Triki, S.; Boukheddaden, K. Interplay between Spin-Crossover and Luminescence in a Multifunctional Single Crystal Iron (II) complex: Towards a New Generation of Molecular Sensors. *Chem. Sci.* **2019**, *10*, 6791-6798.
15. Matsuda, M.; Isozaki, H.; Tajima, H. Reproducible on-off switching of the light emission from the electroluminescent device containing a spin crossover complex. *Thin Solid Films* **2008**, *517*, 1465-1467.
16. Halcrow M. A. (Eds.), Spin-Crossover Materials, Properties and Applications. **2013** John Wiley & Sons Ltd, Oxford, UK.

17. Pittala, N.; Thétiot, F.; Triki, S.; Boukheddaden, K.; Chastanet, G.; Marchivie, M. Cooperative 1D Triazole-Based Spin Crossover Fe^{II} Material With Exceptional Mechanical Resilience. *Chem. Mater*. **2017**, *29*, 490–494.

18. Phan, H.; Hrudka, J. J.; Igimbayeva, D.; Lawson Daku, L. M.; Shatruk, M. A Simple Approach for Predicting the Spin State of Homoleptic Fe(II) Tris-diimine Complexes. *J. Am. Chem. Soc.* **2017**, *139*, 6437-6447.

19. Pittala, N.; Thétiot, F.; Charles, C.; Triki, S.; Boukheddaden, K.; Chastanet, G.; Marchivie, M. An unprecedented trinuclear Fe^{II} triazole-based complex exhibiting a concerted and complete sharp spin transition above room temperature. *Chem. Commun.* **2017**, *53*, 8356-8359.

20. Milin, E.; Patinec, V.; Triki, S.; Bendeif, E.-E.; Pillet, S.; Marchivie, M.; Chastanet, G.; Boukheddaden, K. Elastic Frustration Triggering Photoinduced Hidden Hysteresis and Multistability in a Two-Dimensional Photoswitchable Hofmann-Like Spin-Crossover Metal-Organic Framework. *Inorg. Chem*. **2016**, *55*, 11652-11661.

21. Shatruk, M.; Phan, H.; Chrisostomo, B. A.; Suleimenova, A. Symmetry-breaking structural phase transitions in spin crossover complexes. *Coord. Chem. Rev*. **2015**, *289-290*, 62-73.

22. Atmani, A.; El Hajj, F.; Benmansour, S.; Marchivie, M.; Triki, S.; Conan, F.; Patinec, V.; Handel, H.; Dupouy, G.; Gómez-García, C. J. Guidelines to design new spin crossover materials. *Coord. Chem. Rev.* **2010**, *254*, 1559-1569.

23. El Hajj, F.; Sebki, G.; Patinec, V.; Marchivie, M.; Triki, S.; Handel, H.; Yefsah, S. Macrocycle-based spin-crossover materials. *Inorg. Chem.* **2009**, 48, 10416-10423.

24. N Pittala, N.; Thétiot, F.; Triki, S.; Boukheddaden, K.; Chastanet, G.; Marchivie, M. Cooperative 1D Triazole-Based Spin Crossover Fe^{II} Material With Exceptional Mechanical Resilience. *Chem. Mater.* **2017**, *29*, 490-494.

25. Setifi, F.; Milin, E.; Charles, C.; Thétiot, F.; Triki, S.; Gomez-Garcia, C. G. Spin Crossover Iron(II) Coordination Polymer Chains: Syntheses, Structures, and Magnetic Characterizations of $[Fe(aqin)_2(\mu_2\text{-}M(CN)_4)]$ (M = Ni(II), Pt(II), aqin = Quinolin-8-amine). *Inorg. Chem.* **2014**, *53*, 97-104.

26. Cuza, E.; Motei, R.; Setifi, F.; Bentama, A.; Gómez-García, C. J.; Triki, S. Coordination Isomerism in Spin Crossover (SCO) Materials. *J. Appl. Phys.* **2021**, *129*, 145501.

27. Yamada, M.; Ooidemizu, M.; Ikuta, Y.; Osa, S.; Matsumoto, N.; Iijima, S.; Kojima, M.; Dahan, F.; Tuchagues, J.-P. Interlayer Interaction of Two-Dimensional Layered Spin Crossover Complexes $[Fe^{II}H_3L^{Me}][Fe^{II}L^{Me}]X$ (X^- = ClO_4^-, BF_4^-, PF_6^-, AsF_6^-, and SbF_6^-; H_3L^{Me} = Tris[2-(((2-methylimidazol-4-yl)methylidene)amino)ethyl]amine). *Inorg. Chem.* **2003**, *42*, 8406-8416.

28. Gómez, V.; Sáenz de Pipaón, C.; Maldonado-Illescas, P.; Waerenborgh, J.C.; Martin, E.; Benet-Buchholz, J.; Galán-Mascarós, J.-R. Easy Excited-State Trapping and Record High T_{TIESST} in a Spin-Crossover Polyanionic Fe(II) Trimer. *J. Am. Chem. Soc.* **2015**, *137*, 11924–11927.

29. Hirosawa, N.; Oso, Y.; Ishida, T. Spin crossover and light-induced excited spin-state trapping observed for an iron (II) complex chelated with tripodal tetrakis (2-pyridyl) methane. *Chem. Lett.* **2012**, *41*, 716-718.

30. Yamasaki, M.; Ishida, T. Spin-crossover thermal hysteresis and light-induced effect on iron (II) complexes with tripodal tris (2-pyridyl) methanol. *Polyhedron* **2015**, *85*, 795-799.

31. Yamasaki, M.; Ishida, T. Heating-rate dependence of spin-crossover hysteresis observed in an iron (II) complex having tris (2-pyridyl) methanol. *J. Mater. Chem. C* **2015**, *3*, 7784-7787.

32. Ishida, T.; Kaneto, T.; Yamasaki, M. An iron(II) complex tripodally chelated with 1,1,1-tris(pyridine-2-yl)ethane showing room-temperature spin-crosssover behaviour. *Acta Cryst.* **2016**, *C72*, 797-801.

33. Kashiro, A.; Some, K.; Kobayashi, Y.; Ishida, T. Iron(II) and 1,1,1-Tris(2-pyridyl)nonadecane Complex Showing an Order–Disorder-Type Structural Transition and Spin-Crossover Synchronized over Both Conformers. *Inorg. Chem.* **2019**, *58*, 7672-7676.

34. Cuza, E.; Benmansour, S.; Cosquer, N.; Conan, F.; Pillet, S.; Gómez-García, C. J.; Triki, S. Spin Cross-Over (SCO) Anionic Fe(II) Complexes Based on the Tripodal Ligand Tris(2-pyridyl)ethoxymethane. *Magnetochemistry* **2020**, *6*, 26.

35. Cuza, E.; Mekuimemba, C. D.; Cosquer, N.; Conan, F.; Pillet, S.; Chastanet, C.; Triki, S. Spin Crossover and High-Spin State in Fe(II) Anionic Polymorphs Based on Tripodal Ligands. *Inorg. Chem.* **2021**, doi:10.1021/acs.inorgchem.1c00335

36. White, D. L.; Faller, J. W. Preparation and Reactions of the C_{3v} Ligand Tris(2-pyridyl)methane and Its Derivatives. *Inorg. Chem.* **1982**, *21*, 3119-3122.

37. Jonas, R. T.; Stack, T. D. P. Synthesis and Characterization of a Family of Systematically Varied Tris(2-pyridyl)methoxymethane Ligands: Copper(I) and Copper(II) Complexes. *Inorg. Chem.* **1998**, *37*, 6615-6629.

38. Sorai, M.; Seki,S. Phonon coupled cooperative low-spin $^1A^1 \leftrightarrow$ high-spin $^5T_2$ transition in $[Fe(phen)_2(NCS)_2]$ and $[Fe(phen)_2(NCSe)_2]$ crystals, *J. Pbys. Chm. Solids* **1974**, *35*, 555-570.

39. Brehm, G.; Reiher, M.; Le Guennic, B.; Leibold, M.; Schindler, S.; Heinemann, F. W.; Schneider, S. Investigation of the low-spin to high-spin transition in a novel $[Fe(pmea)(NCS)_2]$ complex by IR and Raman spectroscopy and DFT calculations. *J. Raman Spectrosc.* **2006**, 37: 108-122.

40. Park, Y.; Jung, Y. M.; Sarker, S.; Lee, J.-J.; Lee, Y.; Lee, K.; Oh, J. J.; Joo, S.-W. Temperature-dependent infrared spectrum of $(Bu_4N)_2[Ru(dcbpyH)_2(NCS)_2]$ on nanocrystalline TiO_2 surfaces. *Solar Energy Materials & Solar Cells* **2010**, *94*, 857–864.

41. V. Varma,V.; Fernandes, J.-R. An Infrared Spectroscopic Study of the Low-Spin-High-spin transition in in $Fe_xMn_{1-x}(Phen)_2(NCS)_2$: a Composition-Induced Change in the Order of the Spin-State Transition. *Chem. Phys. Let.* **1990**, *167*, 367-370.

42. Sankar, G.; Thomas, J. M.; Varma, V.; Kulkani, G. U.; Rao, C. N; R. An investigation of the first-order spin-state transition in the $Fe(Phen)_2(NCS)_2$ EXAFS and infrared spectroscopy. *Chem. Phys. Let.* **1996**, *251*, 79-83.

43. Smit, E.; de Waal, D.; Heyns, A.M. The spin-transition complexes $[Fe(Htrz)_3](ClO_4)_2$ and $[Fe(NH_2trz)_3](ClO_4)_2$ I. FT-IR spectra of a low pressure and a low temperature phase transition. *Materials Research Bulletin* **2000**, *35*, 1697–1707.

44. Durand, P.; Pillet, S.; Bendeif, E.-E.; Carteret, C.; Bouazaoui, M.; El Hamzaoui, H.; Capoen, B.; Salmon, L.; Hébert, S.; Ghanbaja, J.; Aranda, L.; Schaniel, D. Room temperature bistability with wide thermal hysteresis in a spin crossover silica nanocomposite. *J. Mater. Chem. C* **2013**, *1*,1933-1942.

45. Bain, G. A.; Berry, J. F. Diamagnetic corrections and Pascal's constants. *J. Chem. Educ.* **2008**, *85*, 532-536.

46. Benmansour, S.; Gómez-Claramunt, P.; Gómez-García, C. G. Effects of water removal on the structure and spin-crossover in an anilato-based compound. *J. Appl. Phys.* 2021, *129*, 123904.